Nucleation and Growth of Microtubules from γ-Tubulin-Functionalized Gold Surfaces

Yi Yang,[†] Pierre A. Deymier,*[,†] Lian Wang,[‡] Roberto Guzman,[‡] James B. Hoying,[§] Heather J. McLaughlin,[||] Shane D. Smith,[†] and Ian N. Jongewaard[||]

Department of Materials Science and Engineering, The University of Arizona, Tucson, Arizona 85721, Department of Chemical and Environmental Engineering, The University of Arizona, Tucson, Arizona 85721, Division of Biomedical Engineering, Arizona Research Laboratories, The University of Arizona, Tucson, Arizona 85724, and Department of Pediatrics, Children's Research Center, The University of Arizona, Tucson, Arizona 85724

Microtubules are protein filaments that are emerging as potential building blocks in manufacturing nanoscale structures and systems such as interconnecting nanowires. Future development in using microtubules necessitates a control of their nucleation and growth. We report the controlled nucleation and growth of microtubules from functionalized gold on a hydrophilic oxidized silicon wafer. The gold substrate is functionalized with γ-tubulin, a natural nucleating agent for microtubule growth. We show that the attached γ-tubulin retains its biological functionality and leads to nucleation and assembly of microtubules from the functionalized gold surface. We also analyze the interplay between the geometry of the nucleating substrates and the morphology of microtubules arrays and networks grown from them. We consider two geometrical arrangements of the substrates: (a) a square lattice of small gold pads on a hydrophilic oxidized silicon wafer and (b) a large flat surface. Fluorescence microscopy and scanning electron microscopy are employed to provide a detailed characterization of the length and morphology of the nucleated and grown microtubules. The observed microtubule morphologies are modeled, analyzed and discussed within the context of reaction−diffusion and nucleation controlled processes.

Introduction

Microtubules (MT) are naturally formed tubular structures, 24 nm in outer diameter and up to many microns in length (*1*). MTs are biopolymers assembled from protein heterodimers containing both α- and β-tubulin. In the presence of the small molecule guanosine triphosphate (GTP), the tubulin heterodimer (Tu-GTP) will self-assemble into the MT structure. The MTs' aspect ratio, chemical polarity, reversibility in assembly, and ability to be metallized by electroless plating (*2*, *3*) make them good candidates to serve as templates for the fabrication of metallic nanowires and other nanoscale systems (*4*). In addition, microtubules can provide biological interactions with a native high specificity (*5*−*7*). The exposure of different tubulin regions at either end of a microtubule (plus/minus end) makes it possible to control MT attachment to substrates in a specific orientation. For instance, Limberis et al. took advantage of the polarity and specificity of biological interactions of MTs to flow-align pregrown MTs immobilized onto a silica substrate using a single-chain antibody that binds only to a portion of α-tubulin exposed at the MT minus end (*8*).

MTs are polarized with a slow-growing end (so-called minus end exposing α-tubulin) and fast-growing end (β-tubulin terminated plus end). The plus end of a MT typically grows at a rate 5−10 times faster than the minus end. In vitro, MTs can be grown from solutions containing high concentrations of purified tubulin (*9*−*15*). Microtubules generated from pure tubulin exist in a dynamic state (called dynamic instability) with net addition of tubulin to the plus end and net removal of tubulin from the minus end. This "treadmilling" effect can be controlled via interaction of the MT with various chemical agents (i.e., microtubule associated proteins (MAP), taxol) resulting in relatively stable MTs (*16*, *17*). In the absence of these agents and for tubulin concentrations below a critical value, C_c, MTs will depolymerize (*18*). Tubulin dimers polymerize into MTs for tubulin concentrations above C_c. At concentrations of tubulin dimmers near C_c, individual MTs exhibit dynamic instability (*19*) and undergo apparently random successive periods of disassembly (catastrophe) and assembly (rescue). The mechanism for transition between a growing state and a shrinking state is generally believed to be associated with hydrolysis of bound GTP when tubulin heterodimers become incorporated within the microtubule structure. Although the process of MT growth is reasonably well understood, in vivo and in vitro MT nucleation is, however, still poorly understood. Within the cell, the minus end is tethered to microtubule-organizing centers (MTOC) such as centrosomes, and the plus end extends into the cytoplasm (*20*). MT assembly is believed to nucleate from the MTOC through interaction with a tubulin isoform, γ-tubulin (*21*−*23*). Research in vitro has shown that γ-tubulin is an essential component in the centrosome for microtubule nucleation (*24*, *25*). Monomeric γ-tubulin and γ-tubulin protein complexes can both nucleate MT. The nucleation time of MTs has been shown to be shorter in the presence of monomeric γ-tubulin (*26*). In vitro, monomeric γ-tubulin behaves as a minus-end-specific protein, with very high binding specificity to the microtubule end. It caps microtubule minus ends and

* To whom correspondence should be addressed. Ph: 520-621-6080. E-mail: deymier@email.arizona.edu.
[†] Department of Materials Science and Engineering.
[‡] Department of Chemical and Environmental Engineering.
[§] Division of Biomedical Engineering, Arizona Research Laboratories.
[||] Department of Pediatrics, Children's Research Center.

10.1021/bp050150j CCC: $33.50
Published on Web 01/07/2006

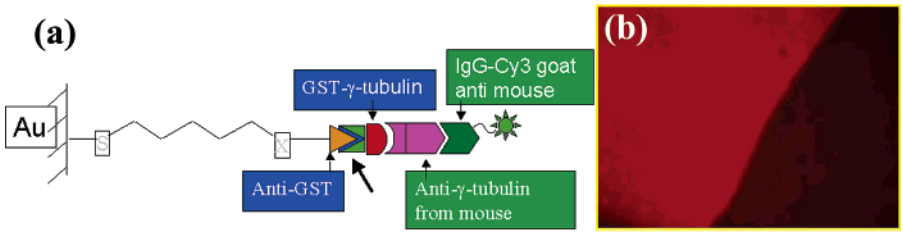

Figure 1. (a) Schematic of functionalized gold surface. S stands for sulfur, X for carboxylic acid. The fusion protein, GST-γ-tubulin, is anchored by a rabbit antibody that specifically binds GST. A mouse monoclonal antibody that recognizes γ-tubulin was then allowed to adhere. That antibody was then recognized by a fluorescent goat anti-mouse antibody (IgG-Cy3) demonstrating the extent of protein assembly. (b) The strong uniform actual fluorescence of the gold electrode (left) on a SiO_2 substrate in the fluorescence microscopy image on the right indicates uniform coverage of the electrode.

catalyzes microtubule nucleation (*26*, *27*). Specific peptides and/or complexes of γ-tubulin have also been identified to serve as binding sites to interact with tubulin heterodimers (*28*−*32*).

The applicability of using MTs as templates for interconnecting devices on microchips necessitates the development of a protocol where MTs can be nucleated and directionally grown from specific sites on the microchip toward some target site elsewhere on that chip. Toward the goal of manufacturing MT-based nanostructures on a silicon wafer, we report here an "in situ" approach consisting of a starting metal pad functionalized with a derivatized MT nucleating complex and surface-driven growth of MTs from the pad. The advantage of this approach lies not only in the immobilization of MTs on the surface of a substrate but more importantly on the unique ability to initiate MT growth from desired sites. In addition, we also report on the effect of the geometry of the substrate on the morphology of the MTs. Based on the premise that MT growth may be influenced by the geometry of the environment, we have conducted additional experiments of MT growth from γ-tubulin-functionalized surfaces with two geometrical arrangements of the substrates, namely, a square lattice of small gold pads (10 μm × 10 μm) on a hydrophilic oxidized silicon wafer and a large flat surface (nearly semi-infinite with respect to the scale of MTs). Fluorescence microscopy and scanning electron microscopy are employed to provide a detailed characterization of the morphology of the nucleated and grown microtubules.

Experimental Methods

MT Nucleating Complex. We have generated a fusion protein consisting of glutathione *S*-transferase (GST) and γ-tubulin to be used as the nucleating agent for the initiation of microtubule growth. The GST-γ-tubulin was developed by first extracting RNA from human cells and using RT-PCR to obtain γ-tubulin. The primers that we used introduced restriction sites at both ends. Additionally, one of the primers created slight changes in codon sequence at the 5′ end; this particular clone could then be used to generate a fusion protein in pGEX-KG. This vector, containing GST followed by a glycine link, was used to generate our fusion protein GST-γ-tubulin. The recombinant protein was then produced in *E. coli* containing the expression construct and it was initially grown in 1 L of LB in the presence of 100 μg/mL ampicillin. When the culture reached an absorbance of 0.9 at 600 nm, 1 mM isopropyl- β-D-thiogalactopyranoside (IPTG) was added to induce the expression of the GST-γ-tubulin. After 3 h, the *E. coli* was concentrated by pelleting using centrifugation for 10 min at 15,000 × *g*. The pellet was then resuspended in 10 mL of PBST and was then placed on ice for 30 min in the presence of lysozyme. Cells were then ruptured using a Polytron three times for 10 s at maximum setting. Centrifugation at 10,000 × *g* for 10 min at 4 °C provided supernatant that was passed through a 1 mL GSTtrap FF column (Amersham Biosciences). A standard protocol was then used to wash unbound proteins from the column and then to elute GST-γ-tubulin using free glutathione. Purity of the final product was analyzed using SDS−PAGE and specific antibody recognition. The final purification contained greater than 80% of a 85 kD protein, the size estimated to be the fusion protein. The recombinant protein was then verified using ELISA with antibodies that recognized specifically either GST or γ-tubulin. The final concentration of GST-γ-tubulin was estimated to be between 4 and 5 μM.

Gold Surface Functionalization. A protein nucleation method for MT growth from gold substrates has been developed based on the self-assembly of reactive alkanethiols together with the engineered fusion protein. Oxidized silicon wafers were patterned with gold electrodes, followed by treatment with piranha solution to clean organic contaminants and to activate the gold surface. An anti-GST antibody was bound to a SAM of carboxylic acid terminated alkanethiols on the gold surface through the carboxylic acid group at the end of the alkyl chains (Figure 1a). Anti-GST is a specific antibody for selective binding of GST attached to recombinant proteins, in our case, the microtubule-nucleating fusion protein, GST-γ-tubulin. Additionally, a specific antibody that binds γ-tubulin is then recognized by a secondary antibody that has a fluorescent tag (IgG-Cy3) and is used to quantify the extent of the formation of the protein assembly. Strong fluorescence from a functionalized gold surface on a SiO_2 substrate coated with the fusion protein indicates that the approach we have developed gives a uniform coverage of the electrode (Figure 1b).

We have also characterized the morphology of the functionalized gold substrate by atomic force microscopy (AFM). Figure 2 reports AFM data of the initial localization of a γ-tubulin-functionalized gold surface and of a pure gold surface. Prior to imaging, the pure gold surface was treated with piranha solution. The gold substrate exhibits some roughness with feature size of approximately 80−100 nm. The γ-tubulin localized surface appears to be morphologically similar to that of the gold substrate, indicating that the nucleating fusion-protein film binds the substrate.

MT Growth. For this study, we used tubulin (>99% pure) prepared from bovine brain extracts and modified with covalently linked fluorescein (Cytoskeleton Inc). The fluorescein-modified tubulin was stored at −70 °C in storage buffer (pH 6.8; 80 mM piperazine-*N*,*N*′-bis[2-ethanesulfonic acid] sequisodium salt (PIPES), 1 mM magnesium chloride ($MgCl_2$); 1 mM ethylene glycol-bis(β-amino-ethyl ether) *N*,*N*,*N*′,*N*′-tetraacetic acid (EGTA), and 1 mM guanosine 5′-triphosphate (GTP)).

In vitro MT assembly was performed in PEM 80 buffer (80 mM PIPES, 1 mM EGTA, 4 mM magnesium chloride ($MgCl_2$), using KOH to adjust PH to 6.9) using a final concentration of

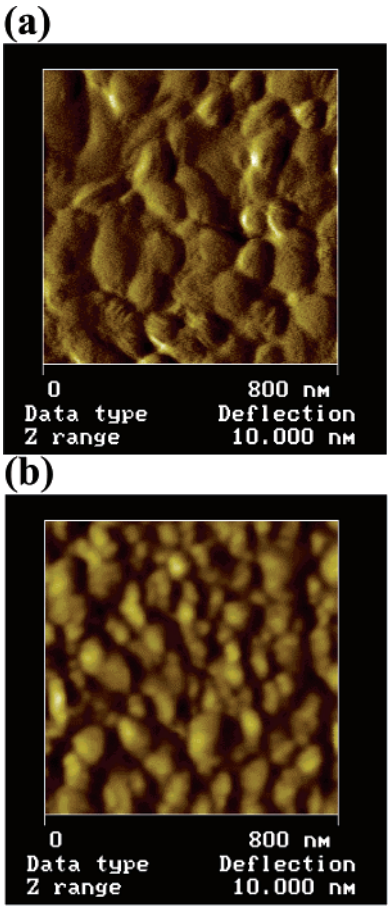

Figure 2. Surface morphology of (a) functionalized gold surface and (b) pure gold surface taken by atomic force microscopy (AFM). The gold surface was treated with piranha solution to remove any undesirable organic contaminant and to activate the gold surface before use. The functionalized gold surface was covered by a layer of GST-γ-tubulin. The γ-tubulin layer conforms to the gold surface.

tubulin at 0.25 mg/mL (2.3×10^{-6} M). Polymerization was initiated by the addition of GTP (final concentration is 0.25 mM) in the presence of taxol (final concentration is 10 μM). To test the specificity of the interaction between MTs and the γ-tubulin-functionalized substrates, we have conducted experiments in which MTs were grown in the presence or absence of the functionalized Au surfaces. In the first case, patterned silicon substrates with functionalized Au pads were immersed into the solution during the polymerization process. The solutions, both with and without substrates, were transferred from an ice bath to a heat bath at 37 °C to promote polymerization for some predetermined amount of time. Because the MT concentration is very high in the solution, we have analyzed the MT growth dynamics in the solution by diluting it 50-fold into PEM 80 buffer and immediately fixing the MTs using the same amount of solution of 3% glutaradehyde for at least 3 min. The solution containing the fixed MTs was transferred onto a poly-L-lysine-coated slide for observation. The microchips were pulled out after polymerization, rinsed with PBS buffer for approximately 10 s, and fixed using methanol (−20 °C) for 3 min. The microtubules both on the glass slide and on the microchips were examined using immunofluorescence microscopy. Detailed structural information was also obtained by scanning electron microscopy (SEM). The samples were prepared by supercritical CO_2 drying after fixing the MTs with glutaradehyde (3%) followed by sputtering a thin film of gold.

Gold Substrates. Two different geometries of gold substrates were used in the study of the effect of the substrate on MT morphology. The gold substrates were patterned on a hydrophilic oxidized silicon wafer. The first substrate is nearly semi-infinite compared to the scale of MTs with dimensions 1.9×3.8 mm^2. The second geometry consists of a square lattice of small gold square pads ($10\ \mu m \times 10\ \mu m$) on a hydrophilic oxidized silicon wafer. The periodicity of the lattice was also 10 μm. The cross sections of the two-types of geometries are illustrated in Figure 3.

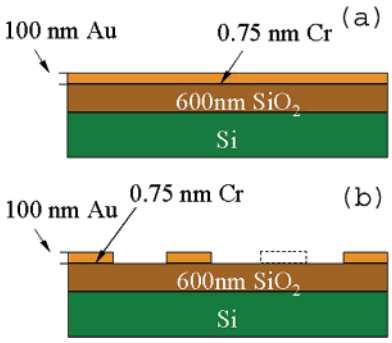

Figure 3. Cross sections of the oxidized silicon substrate patterned with (a) a large gold electrode (1.9×3.8 mm^2) and (b) an array of small gold pads ($10 \times 10\ \mu m^2$); 0.75 nm Cr is used to attach the gold pads onto the silicon dioxide. The thickness of the gold pads is 100 nm.

Results and Discussion

Microtubules were grown in the presence of two different gold surfaces prepared on hydrophilic oxidized silicon wafers. The gold pads on the first sample were functionalized with the GST-γ-tubulin as a nucleation protein. The gold pads on the second sample were not functionalized, and their immersion in a solution of tubulin served as a control experiment. In Figure 4 we report fluorescence microscopy images of typical pads on both samples. Sampling of the solution in which the non-functionalized sample was immersed indicated the presence of numerous MTs in suspension; however, none are to be seen on the surface of the non-functionalized substrate. In contrast the functionalized gold pad appears to be covered with MTs. To rule out direct nonspecific interaction between MTs self-assembled in the solution and the functionalized gold electrodes, we have compared the growth dynamics of MTs grown in solution and of MTs that appear to cover the γ-tubulin-functionalized gold surfaces. Two series of experiments were conducted for different growth times. In the first series we investigated the growth dynamics of the MTs that appear to cover the functionalized gold electrodes. The second series consisted of a study of the growth dynamics of MTs in the absence of functionalized substrate under the same growth conditions. Two polymerization time periods were considered: 5 and 10 min. The length distributions of MTs grown in the presence of a substrate that appear to cover the gold electrodes and the length distribution of MTs nucleated and grown in solution were measured. We report in Figure 5 the length distribution after 5 and 10 min of polymerization. The experiments that lasted 5 min show trends similar to those that lasted twice as much but of course lower values of the average MT lengths. Figure 5a and b show that the functionalized gold pad has a strong influence on the growth dynamics of MTs. The average lengths of MTs grown in solution are approximately 0.62 and 1.11 μm after 5 and 10 min of polymerization, respectively. In the presence of functionalized microchips, the average lengths of MTs on the functionalized gold surfaces increased significantly. Comparing the results of the polymerization with and without functionalized microchips, the average

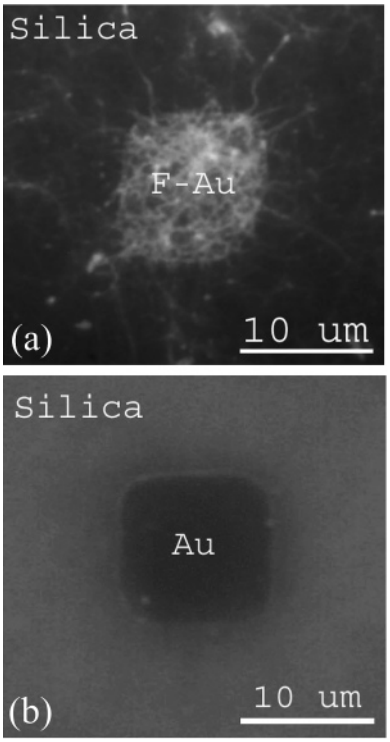

Figure 4. Fluorescence microscopy images of a typical small gold electrode on silica in (a) a sample with functionalized gold electrodes (F-Au) and (b) a sample with non-functionalized electrodes (Au) (cleaned with piranha solution). The immersion time in the tubulin-containing solution is 30 min. Note that in (b) the gold electrode appears relatively dark and the silica peripheral region appears relatively bright compared to (a). This change in contrast is due to the automatic adjustment of the contrast by the digital camera used to take the pictures and the lack of affinity of tubulin dimers for the non-functionalized gold surface.

MT length increased from 0.62 to 1.68 μm for 5 min of polymerization and increased from 1.11 to 3.47 μm for the longer experiments. This result indicates that the γ-tubulin-functionalized gold surface interacts specifically with MTs, by promoting the nucleation of MTs and their subsequent growth.

To verify that MTs growing from the functionalized gold pads are tethered to the γ-tubulin-coated surface, we have conducted real-time observations of MT growth under a fluorescent microscope. For this experiment we have used a large flat functionalized gold substrate. A droplet of solution containing fluorescein-tubulin was placed directly onto the functionalized gold surface for MT assembly and observed using immuno-fluorescence microscopy. By focusing through different focal planes, MTs were found both on the gold surface and in the solution above the surface. The MTs observed in the proximity of the substrate are anchored by one end to the surface. We show in Figure 6 a single MT that appears to be attached by one end to the surface. The microscope is focused on the pad surface thus the segment of the MT nearest to the substrate is in focus. The other end of the MT is blurred and out of focus, indicating that the MT is pointing into the solution. By applying pressure onto the cover slip of the microscope slide, we have induced a shear flow of the solution that drags and aligns the pointing end of the MT in its direction. The end of the MT closest to the substrate does not undergo any displacement showing that the MT is indeed bound to the functionalized gold pad. MTs nucleated and grown from a functionalized surface are shown to be amenable to orientation by fluid flow. Additional post-nucleation and growth observations of flow align MTs are presented in Figure 7. MTs were grown from a large functionalized gold pad for 30 min. Orientation of the MTs results from fluid passing over the surface during the immersion of the sample into the solution containing methanol used for fixing them. All MTs are aligned in the same direction and appear to be bound by one end to the substrate. It can be unarguably assumed that these MTs are bound by their (−) end as it is a known fact that γ-tubulin interacts only with that very one end (*18*, *26*, *27*).

We have calculated the growth rate of surface-nucleated MTs from the data in Figure 5. We cannot estimate a MT growth rate in the case of the polymerization in solution since the time evolution of the MT length distribution may still be rate-limited by homogeneous nucleation during the first 10 min of the experiment. In contrast, assuming that heterogeneous nucleation of MTs from the functionalized surface occurred in the early stages of the experiment, one can estimate the growth rate of the surface-nucleated MT from the time evolution of the MT length distribution between 5 and 10 min of polymerization. This growth rate is approximately 0.36 μm/min. We note that this rate is not the rate of growth of a single microtubule but is the rate of change of the average length of the population of MTs. This rate is representative of an entire population of MTs that undergo concurrent assembly and disassembly. This rate constitutes therefore an underestimate of the rate of growth of a single MT, as indicated by a comparison with the average growth rate of the plus end of individual MTs of 1.25 ± 0.53 μm/min (at our tubulin concentration of 2.3×10^{-6} M) estimated from experimental measurements (*34*).

Quantitative analysis of images such as that of Figure 7a gives a low surface density of surface-nucleation centers originating MTs of approximately 0.92 per 100 μm^2. This is a lower bound since we did not account for MTs shorter than 1 μm in estimating this density. This density gives an estimated area per center nucleating MTs of approximately 108 μm^2, yielding a mean distance between MT-originating nucleating centers of approximately 12 μm. Figure 7b shows that some of the MTs grown from the surface are very long with a very wide distribution (see Figure 8). The average length of the MTs is $22 \pm 17\mu$m. Numerous bright fluorescent dots are observed on the functionalized gold surface. These must be composed of tubulin dimers clustered on the γ-tubulin-functionalized surface. Some of these clusters appear to serve as centers from which one to several MTs originate. We note however that other MTs do not originate from a cluster and appear to have nucleated directly from the functionalized surface (as was also seen in Figure 6). Figure 7 also shows several clusters that are not associated with grown MTs. Figure 8 reports two SEM images of MTs nucleated on the large gold surface with different magnification. In Figure 8a one sees several very long MTs extending out from a cluster. The cluster is magnified in Figure 8b, showing that it contains several short MTs in addition to the very long one observed in Figure 4a. The cluster therefore appears to have the characteristics of a centrosome-like MT nucleation center, which structure enables the initiation and growth of numerous MTs (*35*). In Figure 4c we show a nucleation center (cluster) that does not lead to the growth of long MTs but from which only short MTs (submicron in length) have emerged.

The effect of geometry of the substrate on MT morphology and dynamics is assessed by growing MTs for 30 min from the functionalized square array of gold pads. The gold pads have nucleated a large number of MTs (see Figure 9a). Most MTs grown on a gold pad are no more than approximately 10 μm long, which corresponds not only to the pad dimensions but

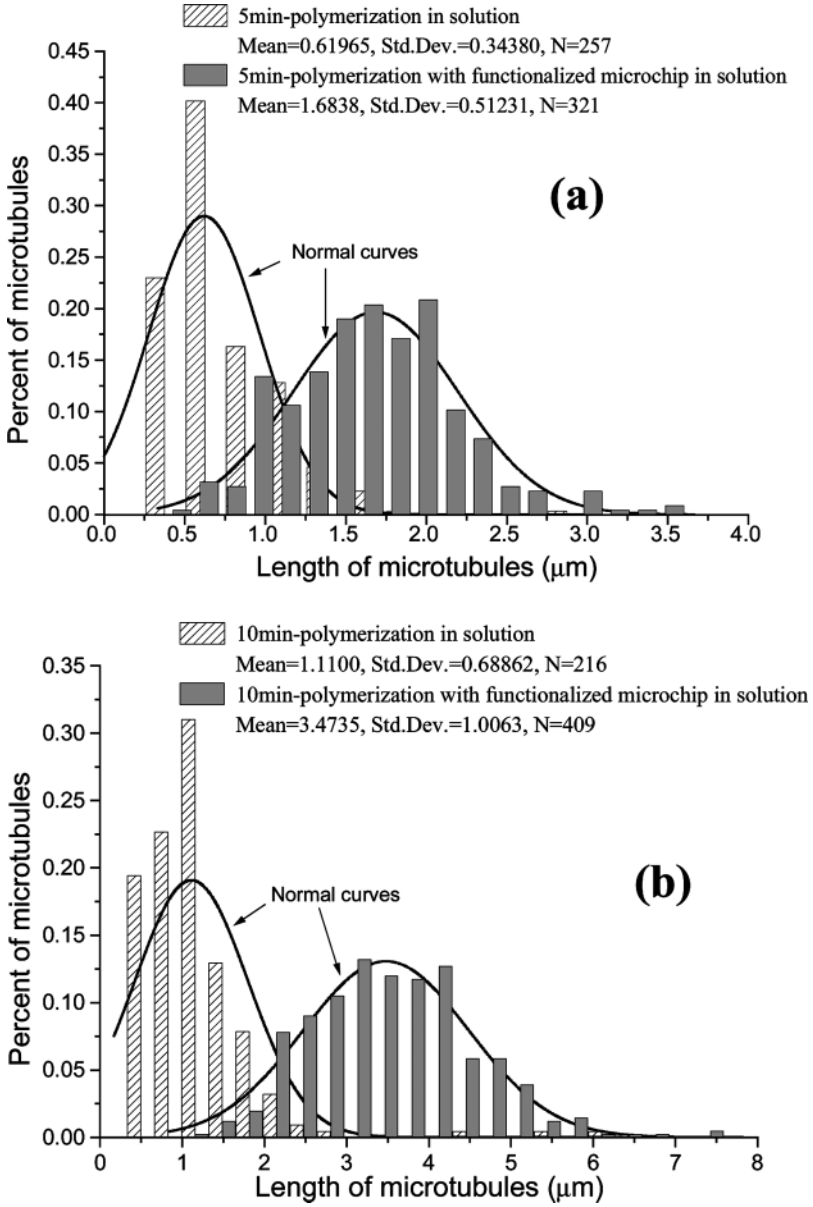

Figure 5. Length distribution of MT polymerized for 5 min (a) and 10 min (b) in solution and from a square array of γ-tubulin-functionalized gold pads.

also to the separation distance between pads. This length is also consistent with the MT growth rate of 0.36 μm/min estimated previously. The surface density of nucleated and grown MTs (in excess of 60 MTs per 100 μm^2) is significantly higher than that of MTs nucleated on the large gold substrate. This observation shows a drastic effect of the geometry of the substrate on MT growth considering that all other conditions are the same. To shed some light on the spatial distribution of MTs grown from the small gold pads, we have aligned them by Marangoni fluid flow (*36*) of the buffer solution over their surface. We start with a microchip covered with a droplet of buffer solution. The volume of the aqueous buffer solution droplet covering the sample was 3 μL at room temperature. When added at one of the sides of the microchip, methanol at −20 °C quickly spreads into the solution (see Figure 10). Although surface tension is a function of temperature and chemical composition, Marangoni flow was induced mainly by the concentration gradient at the solution-methanol interface (temperature effect on the surface tension plays a much lower effect than concentration in this case). The surface tension increases from the side where methanol was added to the opposite side. Marangoni flow occurs from the region with the lowest surface tension to the region with the highest surface tension. The hydrostatic pressure increase in the region with higher surface tension induces a flow along the solution-substrate interface in the direction opposite to the Marangoni flow, orienting the surface-bound MTs in the direction opposite to the direction of spread of the methanol. Once covered by methanol (−20 °C), the MTs are fixed on the functionalized surface.

The fluorescence microscopy image of oriented MTs shown in Figure 9b appears to exhibit slightly brighter contrast near the edges of the square pads that are parallel to the direction of flow compared to the edges perpendicular to the flow. This observation suggests that more MTs may have nucleated near the edges of the pads or that more MTs have been able to grow from the edges of the pads than from the center.

The effect of gold pad geometry on the morphology of surface-nucleated MTs can be discussed in the context of two hypotheses: (a) a difference in the distribution of MT nucleation

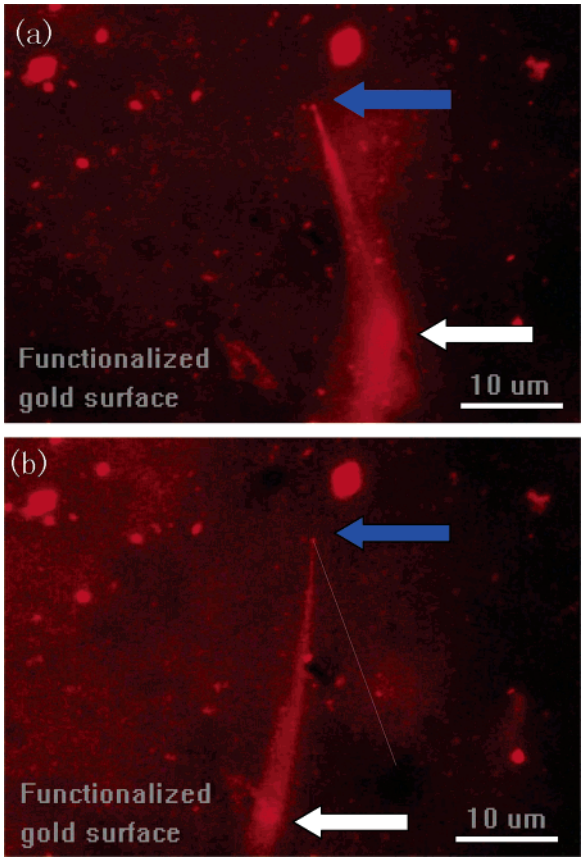

Figure 6. Fluorescence microscope images of a single MT polymerized from a γ-tubulin-functionalized gold surface subjected to a fluid flow. The microscope is focused onto the gold substrate. Both images show that the MT has one end anchored to the surface (indicated by blue arrow) with its other end out of focus pointing into the solution (marked by white arrow). The dotted line in (b) marks the initial position of the MT prior to fluid flow. Bright spots on the surface are believed to be unstructured clusters of fluorescent tubulin.

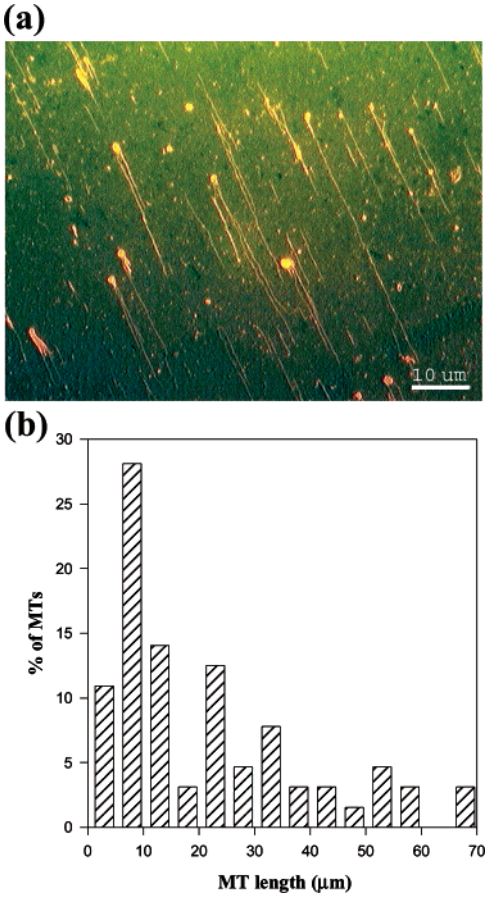

Figure 7. (a) Fluorescent microscope image of MTs grown from a large functionalized gold substrate after 30 min of polymerization at 37 °C subsequently aligned by flowing fluid over the substrate. (b) MT length distribution determined from (a).

centers between the surface and the edges of the γ-tubulin-functionalized pads and/or (b) a reaction−diffusion-limited process that involves competition between the kinetics of MT assembly/disassembly and diffusion of tubulin heterodimers.

Our experiments show that surface-bound γ-tubulin promotes MT nucleation. The difference in the growth behavior of MTs from the surface of the large functionalized gold pad and from the small pads (with strong edge effect) may then be the result of a nonuniform distribution of active nucleating fusion protein. As was stated in the Introduction, the arrangement of γ-tubulin proteins within a nucleation center is critical for effectively initiating nucleation. More favorable arrangements of the γ-tubulin coating may occur at the edge of the pads. A higher density of active nucleation sites at the edge of the gold pads may lead to a higher density of growing microtubules. On the other hand, the existence of nucleation centers on the large gold pad from which only very short MTs have grown (Figure 8c) suggests that other processes may be involved for this geometry. For instance, a reaction−diffusion process (*37*) may play a role in the growth morphology of MTs from the extended functionalized surfaces (nearly semi-infinite geometry).

MT growth is a collective process that is controlled by the nucleation of the MTs, the assembly and disassembly reaction dynamics at the ends of the microtubules and the diffusion of the tubulin monomers. These nonlocal effects may lead to MT growth process that depends on the geometry of the environment in which the MTs grow. The collective nature of MT growth appears in the existence of persistent oscillations in the mass concentration of microtubules (*38*). At high Tu-GTP concentrations, many MTs are nucleated and grown. As the concentration of free Tu-GTP decreases, many MTs transition to a depolymerizating state. The oscillations have been explained as resulting from the time lag between the depolymerization of MTs (i.e., solvation of Tu-GDP) and the exchange of GTP in the solution with liganded GDP to restitute free Tu-GTP that can lead to a new phase of polymerization. Numerous models have been developed to simulate the collective oscillations of microtubules (*38*−*44*). The restitution rate of Tu-GTP has been shown to lead to several types of collective MT growth from monotonic growth to growth followed by shrinkage and stabilization to sustained oscillations to damped oscillations (*48*). Diffusion of tubulin heterodimers has also been shown to play a role in MT organization. MT preparations self-organize spontaneously by reaction−diffusion processes. For instance in vivo and in vitro pattern formation develops in response to a competition between the reaction-controlled dynamics of MT assembly and disassembly and the diffusion of tubulin. When MTs grow from their plus end and disassemble from their minus end, the shrinking leaves behind a chemical trail of high tubulin concentration that leads to preferential growth of other MTs in these regions (*45*−*48*). Diffusion was also shown to lead to self-organization in a model of MTs growing in a finite medium and originating from a centrosome (*49*). The organization forces are again the tubulin concentration gradients, which are generated by the MT assembly/disassembly. Because diffusion may affect the collective growth of MTs, the geometry of the

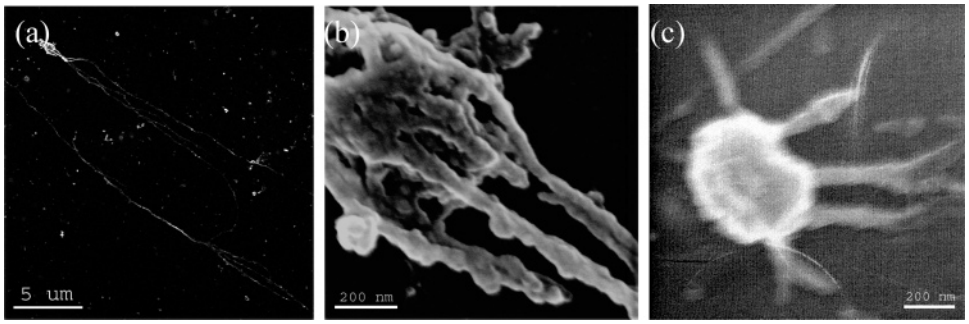

Figure 8. (a) Scanning electron microscopy (SEM) picture of MTs nucleated and aligned on the large functionalized gold substrate, (b) magnified SEM picture of the nucleation center in (a), (c) magnified SEM picture of a nucleation center that gave rise to only short MTs.

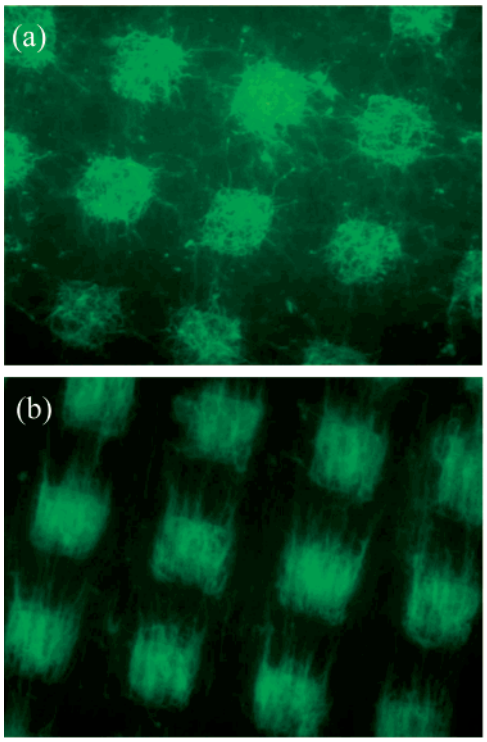

Figure 9. (a) Fluorescent microscope images of MTs grown from the square array of functionalized gold pads after 30 min of polymerization at 37 °C; (b) same as (a) but after alignment of the MTs by flowing fluid over the substrate.

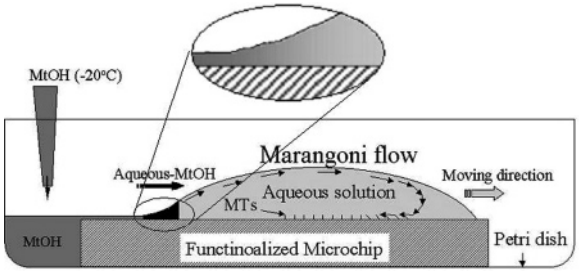

Figure 10. Experimental configuration for aligning MTs using Marangoni flow. Marangoni flow is induced by a gradient in surface tension at the solution-air interface (see text for details). The size of the substrate is exaggerated. Its actual size is 3 mm × 3 mm.

environment in which the MTs grow may control their dynamics and morphology. For example, a semi-infinite geometry model of the growth of MT from a substrate combining reaction dynamics and diffusion shows the existence of a transition between bounded and unbounded growth (*37*). MTs that undergo unbounded growth create a region of tubulin depletion in the vicinity of the surface. As the concentration in the depletion region decreases below the critical concentration, further growth is inhibited in this region leading to the creation of two subpopulations of MT: short MTs undergoing assembly and disassembly near the surface and a group of MT growing nearly continuously beyond the depletion region.

Our observations for the large pad are consistent with such a transition between bounded and unbounded MT growth from the surface.

In an attempt to better understand MT self-organization properties, we have developed a reaction/diffusion model of MT growth. This model is based on the one developed by Glade et al. (*50*). The reactions involved in this model are (a) addition of Tu-GTP to a MT, (b) dissociation of a MT and rejection of guanosine diphosphate (GDP)-liganded tubulin (Tu-GDP) into the solution, and (c) regeneration of Tu-GDP into Tu-GTP. The dynamics of MT assembly and disassembly are based on a cap model whereof Tu-GTP embedded within a microtubule hydrolyses to Tu-GDP. A growing microtubule is thus composed of a Tu-GTP cap of newly added Tu-GTP heterodimers and a core of Tu-GDP. The Tu-GTP cap of a MT is assumed to hydrolyze into the Tu-GDP body at a constant rate. As a consequence of these reactions, local concentrations of Tu-GTP and Tu-GDP may change in the vicinity of assembling and disassembling MTs. The concentrations of Tu-GTP and Tu-GDP are also modified by diffusion. We assume that Tu-GTP and Tu-GDP diffuse in the solution independently of each other. We use the same reaction rate constants and diffusion coefficients as those reported in ref 50.

For the purpose of our study, we have extended Glade et al.'s model to three dimensions. We employ a finite difference scheme to solve the diffusion equation on a three-dimensional square grid with grid spacing of 1 μm. The diffusion equation and reaction kinetics are solved numerically at time intervals of 0.01 s. The bottom face of the simulation cell represents a solid surface, part of which can be functionalized with a predetermined number of MT nucleation centers arranged on some two-dimensional array. Periodic boundary conditions (PBC) are imposed in the plane parallel to the solid surface. The concentration of Tu-GTP is held constant on the uppermost surface of the grid, to simulate a large quantity of solution without making the grid excessively large in the direction perpendicular to the solid surface. To avoid any artifact due to this latter boundary condition, calculations are stopped when a MT grows to a length of 2/3 of the height of the grid in the direction normal to the solid surface. We impose a zero diffusion gradient at the solid surface. The top and bottom surfaces of the grid are separated by a distance of 50 μm. Initially, the entire grid is assigned a uniform concentration of Tu-GTP. Microtubules are only allowed to nucleate on the array of nucleation centers. We use an even distribution of nucleation sites (one per μm^2) to ensure that any self-organization was due to

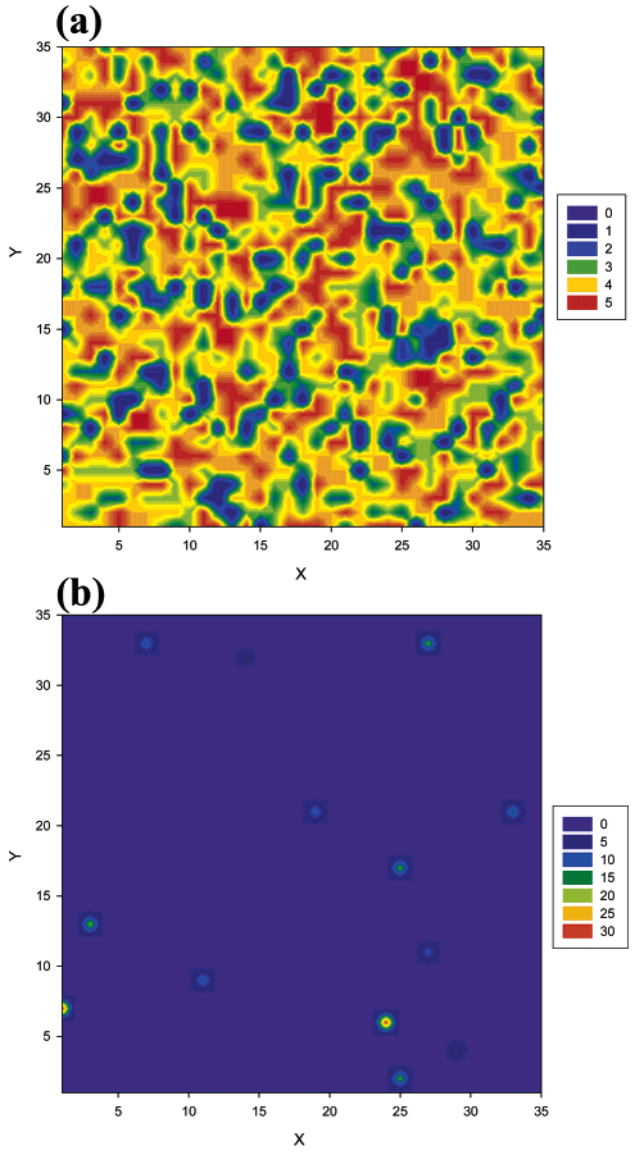

Figure 11. Color contour maps of the length of simulated MT nucleated on a solid surface with a uniform distribution of nucleation centers. The solid surface is composed of 35 × 35 grid sites all nucleation centers. (a) coresponds to early times and (b) to the long time steady-state regime. All dimensions are in μm including the scale of colors corresponding to MT lengths. The initial tubulin concentration is 8 mg/mL.

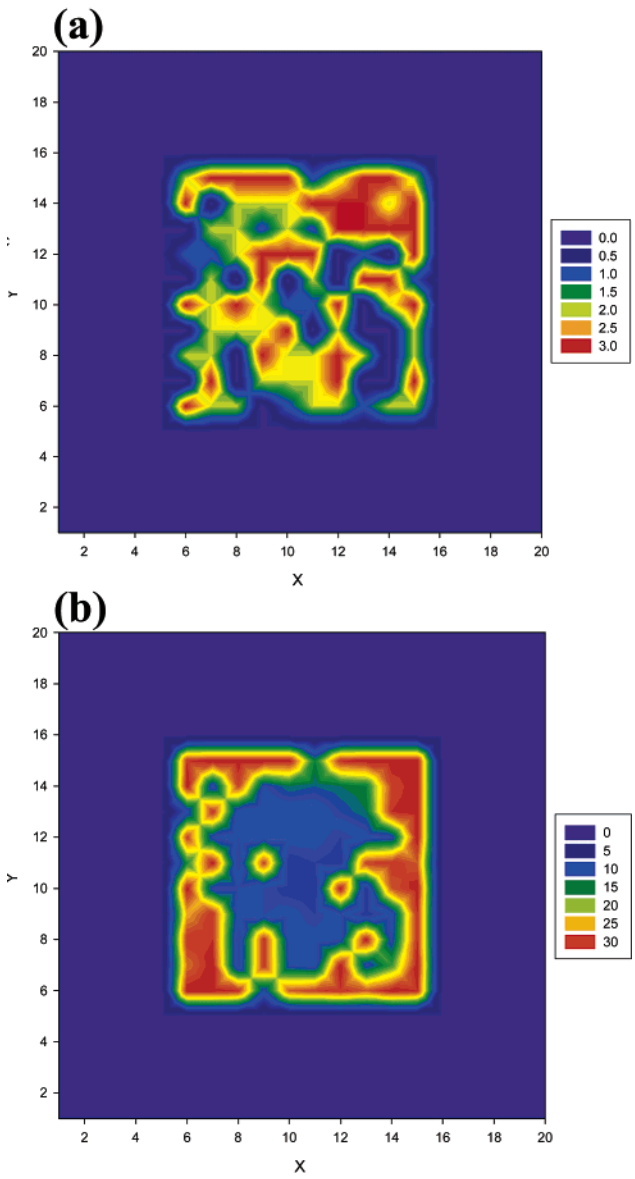

Figure 12. Color contour maps of the length of simulated MT nucleated on a solid surface with a nonuniform distribution of nucleation centers. The solid surface is composed of 20 × 20 grid sites with only the central 10 × 10 grid sites being nucleation centers; (a) corresponds to early times and (b) to the long time steady-state regime. All dimensions are in μm including the scale of colors corresponding to MT lengths. The initial tubulin concentration is 5 mg/mL.

competition between reaction dynamics and diffusion and not to uneven spacing of nucleation sites. A nucleation site may initiate the growth of a MT based on a probability function depending linearly on Tu-GTP concentration with a minimum concentration for nucleation of 2.3×10^{-3}mg/mL. At that minimum concentration the probability for nucleation is 16%. After nucleation, MT growth is constrained to occur in the direction perpendicular to the solid surface.

Two geometries of the solid surface are considered. In the first one, the bottom solid surface is composed of 35 × 35 grid sites and every grid site is also a nucleation site. Due to the PBC, this system models an infinite functionalized surface with a uniform distribution of nucleation sites. The second system models the square array of gold pads. The bottom solid surface is composed of 20 × 20 grid sites with the 10 × 10 central sites consisting of nucleation sites (i.e., nucleation centers on the model pad are distributed uniformly). Again, PBC repeats this arrangement in two directions, thus mimicking the periodic square array of gold pads. To observe MT growth in these models comparable to our experimental observations, we have used an initial Tu-GTP concentration of 8 mg/mL. This concentration is significantly larger than the one used in our experiments but this value is constrained by the choice of rate constants of Dale et al. (*50*). Dale's model does not consider the effect of taxol on the dynamics of microtubule. In that model, the growth velocity of MTs is parametrized to the critical concentration of pure tubulin. It is known from experiments that the dynamics of MT in solutions containing taxol still involves assembly and disassembly events with, however, a significantly lower critical concentration (*51*, *52*). To verify the validity of Dale's model in describing qualitatively our experiments, we have conducted several calculations in which the MT growth velocity of the model was reparametrized to a lower critical concentration. With a lower critical concentration parameter, the model produces morphologies similar to those

obtained without reparametrization but at significantly lower initial Tu-GTP concentration. This shows that in accord with our experimental observations, mimicking the effect of taxol by lowering the critical concentration parameter and consequently the initial TU-GTP concentration does not change the dynamics of the MT self-organization. Consequently, we use Dale's original model for qualitative comparison with our experiments. Figure 11 shows two snapshots in the time evolution of MTs nucleating from the 35×35 grid with uniform distribution of nucleation sites. Early on, every site nucleates a MT that grows to a few micrometers in length. As time proceeds, these MTs deplete the solution in the vicinity of the solid surface and disassemble. After that time only a few MTs that have lengths exceeding the thickness of the depleted region encounter enough Tu-GTP to continue to grow. The steady-state morphology of the simulated system resembles strikingly the morphology observed experimentally in Figure 7. In contrast, the simulation of the functionalized small square pad at an initial Tu-GTP concentration of 8 mg/mL started with a uniform nucleation and growth of MTs over the entire electrode. We report in Figure 12, the more interesting case of nucleation and growth from a functionalized small square pad with a lower initial concentration of 5 mg/mL. The short time state of the surface consists of a reasonably uniform distribution of short MTs nucleated from the functionalized surface, comparable to that of the early state of the large system in Figure 11a. The steady state morphology, however, diverges from the uniformity of the MT length but evolves toward MT growing only along the edges of the pad with a MT-free center. These observation are qualitative similar to the experimental observation of Figure 9. These calculations show that the morphological difference observed experimentally may be explained on the basis of a reaction/diffusion process alone without calling upon a hypothesis of nonuniformity of the distribution of MT nucleation sites on the functionalized gold pads.

Conclusions

We have been able to functionalize gold surfaces with a MT nucleating protein, namely, γ-tubulin. We have also shown that the surface-bound γ-tubulin retains its biological ability to nucleate MTs. The dynamics of MTs grown from a γ-tubulin-functionalized surface is drastically different from that of MT grown from a solution, showing that the functionalized surface interacts specifically with the MTs. MTs grown in the presence of functionalized substrates are tethered to the surface by one end. This end is believed to be the minus end of the MTs.

We have observed that MTs nucleated from a large gold pad and from an array of small gold pads exhibit very different morphologies. MTs grown from an extended pad are often long (many exceed 20 μm in length) and generously spaced (approximately 12 μm). In contrast the length of MTs nucleated on the array of small gold pads does not exceed the periodicity of the array ($\sim$10 μm). The surface density of MTs is nearly 2 orders of magnitude larger in the latter case than in the former. We demonstrate that the observed morphologies can result from competition between reaction dynamics of MT growth and tubulin diffusion.

Acknowledgment

We acknowledge financial support from the National Science Foundation (grant 0303863). We thank Dr. Olgierd A. Palusinski for help in preparing gold patterned microchips and Faith R. Archer for image processing expertise.

References and Notes

(1) Schuyler, S. C.; Pellman, D. Microtubule 'plus-end-tracking proteins': the end is just the beginning. *Cell* **2001**, *105* (4), 421−424.

(2) Kirsch, R.; Mertig, M.; Pompe, W.; Wahl, R.; Sadowske, G.; Unger, E. Three-dimensional metallization of microtubules. *Thin Solid Films* **1997**, *305*, 248−253.

(3) Yang, Y.; Constance, B. H.; Deymier, P. A.; Hoying, J.; Raghavan, S.; Zelinski, B. J. J. Electroless metal plating of microtubules: effect of microtubule-associated proteins. *J. Mater. Sci.* **2004**, *39*, 1927−1933.

(4) Mertig, M.; Kirsch, R.; Pompe, W. Biomolecular approach to nanotube fabrication. *Appl. Phys. A* **1998**, *66*, S723−S727.

(5) Whaley, S. R.; English, D. S.; Hu, E. L.; Barbara, P. F.; Belcher, A. M. Selection of peptides with semiconductor binding specificity for directed nanocrystal assembly. *Nature* **2000**, *405*, 665−668.

(6) Sarikaya, M.; Tamerler, C.; Jen, A. K. Y.; et al. Molecular biomimetics: nanotechnology through biology. *Nat. Mater.* **2003**, *2* (9), 577−585.

(7) Antikainen, N. M.; Martin, S. F. Altering protein specificity: techniques and applications. *Bioorg. Med. Chem.* **2005**, *13* (8), 2701−2716.

(8) Limberis, L.; Magda, J. J.; Stewart, R. J. Polarized alignment and surface immobilization of microtubules for kinesin-powered nanodevices. *Nano Lett.* **2001**, *1* (5), 277−280.

(9) Johnson, K. A.; Borisy, G. G. Kinetic analysis of microtubule self-assembly in vitro. *J. Mol. Biol.* **1977**, *117*, 1−31.

(10) Bayley, P. M.; Martin, S. R. Inhibition of microtubule elongation by GDP. *Biochem. Biophys. Res. Commun.* **1986**, *137* (1), 351−358.

(11) Caplow, M.; Shanks, J.; Breidenbach, S.; Ruhlen, R. L. Kinetics and mechanism of microtubule length changes by dynamic instability. *J. Biol. Chem.* **1988**, *263* (22), 10943−10951.

(12) Simon, J. R.; Salmon, E. D. The structure of microtubule ends during the elongation and shortening phases of dynamic instability examined by negative-stain electron microscopy. *J. Cell Sci.* **1990**, *96* (4), 571−582.

(13) Kowalski, R. J.; Williams, R. C., Jr. Microtubule-associated protein 2 alters the dynamic properties of microtubule assembly and disassembly. *J. Biol. Chem.* **1993**, *268* (13), 9847−9855.

(14) Marx, A.; Mandelkow, E. A model of microtubule oscillations. *Eur. Biophys. J.* **1994**, *22* (6), 405−421.

(15) Caudron, N.; Valiron, O.; Usson, Y.; Valiron, P.; Job, D. A reassessment of the factors affecting microtubule assembly and disassembly in vitro. *J. Mol. Biol.* **2000**, *297* (1), 211−220.

(16) Kinoshita, K.; Arnal, I.; Desai, A.; Drechsel, D. N.; Hyman, A. A. Reconstitution of physiological microtubule dynamics using purified components. *Science* **2001**, *294*, 1340−1343.

(17) Arnal, I.; Wade, R. H. How does taxol stabilize microtubules? *Curr. Biol.* **1995**, *5*, 900−908.

(18) Lodish, H.; Berk, A.; Zipuski, S. L.; Matsudaira, P.; Baltimore, D.; Darnell, J. *Molecular Cell Biology*, 4th ed.; Freeman: New York, 2000.

(19) Mitchison, T.; Kirschner, M. Microtubule assembly nucleated by isolated centrosomes. *Nature* **1984**, *312*, 237−242.

(20) Job, D.; Valiron, O.; Oakley, B. Microtubule nucleation. *Curr. Opin. Cell Biol.* **2003**, *15* (1), 111−117.

(21) Moritz, M.; Zheng, Y.; Alberts, B. M.; Oegema, K. Recruitment of the gamma-tubulin ring complex to Drosophila salt-stripped centrosome scaffolds. *J. Cell Biol.* **1998**, *142*, 775−786.

(22) Schnackenberg, B. J.; Khodjakov, A.; Rieder, C. L.; Palazzo, R. E. The disassembly and reassembly of functional centrosomes in vitro. *Proc. Natl. Acad. Sci. U.S.A.* **1998**, *95*, 9295−3900.

(23) Gunawardane, R. N.; Lizarraga, S. B.; Wiese, C.; Wilde, A.; Zheng, Y. Gamma-Tubulin complexes and their role in microtubule nucleation. *Curr. Top. Dev. Biol.* **2000**, *49*, 55−73.

(24) Felix, M. A.; Antony, C.; Wright, M.; Maro, B. Centrosome assembly in vitro: role of gamma-tubulin recruitment in Xenopus sperm aster formation. *J. Cell Biol.* **1994**, *124*, 19−31.

(25) Stearns, T.; Kirschner, M. In vitro reconstitution of centrosome assembly and function: the central role of gamma-tubulin. *Cell* **1994**, *76*, 623−637.

(26) Leguy, R.; Melki, R.; Pantaloni, D.; Carlier, M. F. Monomeric gamma-tubulin nucleates microtubules. *J. Biol. Chem.* **2000**, *275* (29), 21975−21980.
(27) Li, Q.; Joshi, H. C.; Gamma-tubulin is a minus end-specific microtubule binding protein. *J. Cell Biol.* **1995**, *131*, 207−214.
(28) Llanos, R.; Chevrier, V.; Ronjat, M.; Meurer-Grob, P.; Martinez, P.; Frank, R.; Bornens, M.; Wade, R. H.; Wehland, J.; Job, D. Tubulin binding sites on gamma-tubulin: identification and molecular characterization. *Biochemistry* **1999**, *38*, 15712−15720.
(29) Fuller, S. D.; Gowen, B. E.; Reinsch, S.; Sawyer, A.; Buendia, B.; Wepf, R.; Karsenti, E. The core of the mammalian centriole contains gamma-tubulin. *Curr. Biol.* **1995**, *5* (12), 1384−1393.
(30) Moritz, M.; Braunfeld, M. B.; Sedat, J. W.; Alberts, B.; Agard, D. A. Microtubule nucleation by g-tubulin-containing rings in the centrosome. *Nature (London)* **1995**, *378* (6557), 638−640.
(31) Wiese, C.; Zheng, Y. A new function for the g -tubulin complex as a microtubule minus-end cap. *Nat. Cell Biol.* **2000**, *3*, 358−364.
(32) Oegema, K.; Wiese, C.; Martin, O. C.; Milligan, R. A.; Iwamatsu, A.; Mitchison, T. J.; Zheng, Y. Characterization of two related Drosophila gamma-tubulin complexes that differ in their ability to nucleate microtubules. *J. Cell Biol.* **1999**, *144*, 721−733.
(33) Heald, R.; Tournebize, R.; Blank, T.; Sandaltzopoulos, R.; Becker, P.; Hyman, A.; Karsenti, E. Self-organization of microtubules into bipolar spindles around artificial chromosomes in Xenopus egg extracts. *Nature* **1996**, *382*, 420−425.
(34) Pedigo, S.; Williams, R. C. Concentration dependence of variability in growth rates of microtubules. *Biophys. J.* **2002**, *83*, 1809−1819.
(35) Bornens, M. Centrosome composition and microtubule anchoring mechanisms. *Curr. Opin. in Cell Biol.* **2002**, *14*, 25−34.
(36) Velarde, M. G. Drops, liquid layers and the Marangoni effect. *Philos. Trans. R. Soc. London, Ser. A* **1998**, *356* (1739), 829−844.
(37) Dogterom M.; Leibler, S. Physical aspects of the growth and regulation of microtubules structures. *Phys. Rev. Lett.* **1993**, *70*, 1347−1350.
(38) Tao, Y. C.; Peskin, C. S. Simulating the role of microtubules in depolymerization-driven transport: a Monte Carlo approach. *Biophys. J.* **1998**, *75*, 1529−1540.
(39) Carlier, M. F.; Melki, R.; Pantaloni, D.; Hill, T. L.; Chen, Y. Synchronous oscillations in microtubule polymerization. *Proc. Natl. Acad. Sci. U.S.A.* **1987**, *84*, 5257−5261.
(40) Chen, Y.; Hill, T. L. Theoretical studies on oscillations in microtubule polymerization. *Proc. Natl. Acad. Sci. U.S.A.* **1987**, *84*, 8419−8423.
(41) Houchmandzadeh, B.; Vallade, M. Collective oscillations in microtubule growth. *Phys. Rev. E* **1996**, *53*, 6320−6324.
(42) Jobs, E.; Wolf, D. E.; Flyvbjerg, H. Modeling microtubule oscillations. *Phys. Rev. Lett.* **1997**, *79*, 519−522.
(43) Hammele, M.; Zimmermann, W. Modeling oscillatory microtubule-polymerization. *Phys. Rev. E* **2003**, *67*, 021903.
(44) Marx, A.; Mandelkow, E. A model of microtubule oscillations. *Eur. Biophys. J.* **1994**, *22*, 405−421.
(45) Glade, N.; Demongeot, J.; Tabony, J. Comparison of reaction−diffusion simulations with experiment in self-organised microtubule solutions. *C. R. Biol.* **2002**, *325*, 283−294.
(46) Tabony, J.; Glade, N.; Demongeot, J.; Papaseit, C. Biological self-organization by way of microtubule reaction−diffusion process. *Langmuir* **2002**, *18*, 7196−7207.
(47) Tabony J.; Job, D. Spatial structures in microtubular solutions requiring a sustained energy source. *Nature* **1990**, *346*, 448−451.
(48) Papaseit, C.; Vuillard, L.; Tabony, J. Reaction−diffusion microtubule concentration patterns occur during biological morphogenesis. *Biophys. Chem.* **1999**, *79*, 33−39.
(49) Robert, C.; Bouchiba, M.; Margolis, R. L.; Job, D. Self-organization of the microtubule network. A diffusion based model. *Biol. Cell* **1990**, *68*, 177−181.
(50) Glade, N.; Demongeot J.; Tabony J. Numerical simulations of microtubule self-organization by reaction and diffusion. *Acta Biotheor.* **2002**, *50*, 239−268.
(51) Schilstra, M. J.; Bayley, P. M.; Martin, S. R. The effect of solution composition on microtubule dynamic instability. *Biochem. J.* **1991**, *277*, 839−847.
(52) Ganesh, T.; Guza, R. C.; Bane, S.; Ravindra, R.; Shanker, N.; Lakdawala, A. S.; Snyder, J. P.; Kingston, D. G. I. The bioactive taxol conformation on β-tubulin: experimental evidence from highly active constrained analogues, *Proc. Natl. Acad. Sci.* **2004**, *101*, 10006−10011.

Accepted for publication December 9, 2005.

BP050150J